Research Article | Vol. 29, No. 22 / 25 Oct 2021 / Optics Express 36915
Optics EXPRESS

Carrier-envelope offset frequency dynamics of a 10-GHz modelocked laser based on cascaded quadratic nonlinearities

L. M. KRÜGER,* S. L. CAMENZIND, C. R. PHILLIPS, AND U. KELLER

Department of Physics, Institute for Quantum Electronics, ETH Zurich, CH-8093 Zurich, Switzerland
*lkrueger@phys.ethz.ch

Abstract: Cascaded quadratic nonlinearities from phase-mismatched second-harmonic generation build the foundation for robust soliton modelocking in straight-cavity laser configurations by providing a tunable and self-defocusing nonlinearity. The frequency dependence of the loss-related part of the corresponding nonlinear response function causes a power-dependent self-frequency shift (SFS). In this paper, we develop a simple analytical model for the SFS-induced changes on the carrier-envelope offset frequency (f_{CEO}) and experimentally investigate the static and dynamic f_{CEO} dependence on pump power. We find good agreement with the measured dependence of f_{CEO} on laser output power, showing a broad f_{CEO} tuning capability from zero up to the pulse repetition rate. Moreover, we stabilize the relative intensity noise to the −157 dBc/Hz level leading to a tenfold reduction in f_{CEO}-linewidth.

1. Introduction

Optical frequency combs (OFCs) [1–3] with line spacings of several gigahertz from passively modelocked lasers [4–10] are attractive sources for applications that require easy access to individual comb lines or for trace-gas spectroscopy [11–13]. These systems can produce high average power and femtosecond pulses with low-noise performance [14–16]. In recent years, dual-comb modelocking [17–20] and dual-comb spectroscopy [21–23] gained a lot of attraction due to their mechanical simplicity, high-speed acquisition, high sensitivity, and accuracy. Typically, the frequency resolution of dual-comb spectroscopy is limited by the comb mode spacing but can be increased to the intrinsic comb mode linewidth by interleaving slightly shifted spectra [24–26]. This can be achieved by acting on either of the two comb parameters, *i.e.* the spacing between two comb modes, given by the pulse repetition rate (f_{rep}) or the offset of the first comb tooth with respect to zero, called the carrier-envelope offset frequency (f_{CEO}). The absolute comb mode of an OFC is given by $f_{CEO} + mf_{rep}$, with m being the comb line number. Since f_{CEO} affects all comb modes equally it is the preferred sweeping parameter for spectrally interleaved dual-comb spectroscopy. A tuning range of f_{CEO} over $f_{rep}/2$ is required to fully cover the gap between comb modes. Typically, such broad tuning of f_{CEO} in laser-based OFCs cannot be covered by pump power modulations and requires mechanical translation of intracavity parts. However, we have recently demonstrated broad f_{CEO} tuning over a range from zero up to f_{rep} with pump power in a new type of laser architecture [27,28] based on cascaded quadratic nonlinearity (CQN) [29] from phase-mismatched second harmonic generation (SHG).

Stable femtosecond soliton modelocking [30] results from a balance between self-phase modulation (SPM) and group delay dispersion (GDD). In the infrared wavelength region, SPM is typically obtained from the intrinsic third-order electronic nonlinear susceptibility of wide bandgap materials [31] and balanced with engineered negative GDD from dispersion compensating optics. However, since the pulse energy scales inversely with f_{rep}, the relatively weak nonlinearity of these materials makes it increasingly difficult to obtain sufficient SPM to

#441393 https://doi.org/10.1364/OE.441393
Journal © 2021 Received 24 Aug 2021; revised 10 Oct 2021; accepted 11 Oct 2021; published 22 Oct 2021

Optics EXPRESS

support stable pulse formation for several gigahertz OFCs. In addition, the long upper state lifetimes and low cross-sections of gain media used for many solid-state lasers cause Q-switching instabilities for power levels below the threshold for stable continuous-wave (cw) modelocking [32]. The randomly occurring high-intensity spikes during Q-switching in combination with the self-focusing Kerr-lens resulting from the positive nonlinear refractive index can easily reach the damage threshold of intracavity optical components [33]. The challenges involved in gigahertz OFCs based on watt-level modelocked solid-state lasers can be overcome by introducing an engineerable negative nonlinear response obtained from a CQN. The associated defocusing nonlinearity in combination with a semiconductor saturable absorber mirror (SESAM) [34] allows for a simple straight-cavity architecture that is well suited for watt-level femtosecond modelocked lasers with pulse repetition rates exceeding 10 GHz [27,28].

Precise control of the frequency comb parameters, *i.e.* f_{rep} and f_{CEO}, is required for many frequency comb applications. Commonly, the spacing of the OFC is stabilized by detecting f_{rep} with a sufficiently fast photodiode and acting on the cavity length by modulating a mirror with a piezoelectric element. The second parameter cannot be detected directly with a photodiode since the pulse energy is not modulated at f_{CEO}. Instead, one has to rely on the beating of optical frequencies with either a stable optical reference or another comb tooth. The latter technique is most commonly implemented in f-to-$2f$ detection schemes, which require an octave-spanning spectrum [1]. However, the low pulse energy and limited peak power make it increasingly challenging for high repetition rate lasers to generate sufficient nonlinear broadening for coherent octave-spanning supercontinuum generation (SCG). We recently demonstrated the first self-referenced f_{CEO} detection of a diode-pumped SESAM-modelocked laser with a 10-GHz straight-cavity architecture. This was achieved by combining SCG in a highly efficient silicon nitride (Si_3N_4) waveguide [16,35] with SHG in a reverse proton-exchange periodically poled lithium niobate (RPE-PPLN) waveguide [36] for f-to-$2f$ interferometry. Stabilizing f_{CEO} can be achieved by acting on the pump current and hence the pump power. The exact transfer function of pump modulation to f_{CEO} depends on various laser parameters and has been studied for different types of solid-state and fiber lasers [37–40].

In this paper, we present the first analytical and experimental investigation of f_{CEO} dynamics of a 10-GHz straight cavity laser architecture based on defocusing CQNs. In the first part, we develop an analytical model to describe the quasi-static dependence of f_{CEO} on laser output power (P_{avg}) under the presence of a SFS. In the second part, we characterize the static and dynamic f_{CEO} dependence on P_{avg}. We find good agreement between our model and the measured broad tuning behavior of f_{CEO} from zero up to f_{rep}. Further, we measured the dynamic f_{CEO} response to pump current modulations and the f_{CEO} frequency noise. We observed a significant reduction in the out-of-loop f_{CEO} frequency noise by stabilizing the average output power of the laser, validating the strong coupling predicted by our model. Our results represent the first analytical and experimental investigation of f_{CEO} dynamics in CQN-modelocked lasers.

2. Analysis of f_{CEO} changes induced by a self-frequency shift

Consider a laser pulse propagating through a hypothetical free-space medium having different group (v_{g}) and phase velocities (v_{p}) but no group delay dispersion. As a consequence, this pulse experiences a change in the carrier-envelope phase (CEP) [41] that equates to:

$$\Delta(\phi_{\mathrm{CEP}}) = \omega \left(\frac{1}{v_{\mathrm{p}}} - \frac{1}{v_{\mathrm{g}}} \right) L. \tag{1}$$

For a system free of dispersion and nonlinearity, there is no change in pulse shape and this relation should capture the full behavior. The equation also assumes that $\Delta(\phi_{\mathrm{CEP}})$ has the same sign as the propagation phase $k \cdot L$. The reason for using this definition is that the two types of pure

Optics EXPRESS

phases ($k \cdot L$ and CEP) add without a minus sign. The phase of the electric field envelope, using a carrier term of $\exp(i\omega t - ikz)$ convention, would pick up a minus sign relative to these phases.

For systems involving soliton formation, there is a balance between group delay dispersion (ϕ_{GDD}) and the nonlinear phase shift arising from SPM (ϕ_{SPM}). Consequently, the soliton pulse maintains a fixed pulse shape up to a constant phase (ϕ_{soliton}), so its CEP shift at different positions can be meaningfully compared without having to consider changes in pulse shape. Under these conditions, the constant phase acquired by the pulse amounts to half the nonlinear phase shift that the peak of the pulse would experience and can be expressed in terms of GDD via the soliton formation condition [42]:

$$\phi_{\mathrm{soliton}} = \frac{\phi_{\mathrm{SPM}}}{2} = \frac{\phi_{\mathrm{GDD}}}{2} = -\frac{\mathrm{GDD}}{2{T_0}^2}. \tag{2}$$

In the context of a modelocked laser cavity, the GDD term corresponds to the total cavity round trip group delay dispersion, T_0 is the soliton pulse width and the full-width half maximum (FWHM) pulse duration would equate to $\tau_{\mathrm{FWHM}} = 2 \cdot \cosh^{-1}\left(\sqrt{2}\right) \cdot T_0$. We neglect the influence of soliton self-frequency shift effects on this phase shift because we consider cavity-based systems in which the soliton frequency is not changing versus propagation, but only versus some static system parameter like the average power and cavity length. Under these assumptions, we can express the CEP changes for a laser cavity of total length $2L$ with a cavity round trip time $T_{\mathrm{rt}} = \int_0^{2L} \left(\frac{dk}{d\omega}\right) dz$:

$$\begin{aligned}\Delta(\phi_{\mathrm{CEP}}) &= \phi_{\mathrm{soliton}}(\omega_{sol}) + \int_0^{2L} \left(k(\omega_{sol}) - \omega_{sol} \left(\frac{dk}{d\omega}\right)\Big|_{\omega_{sol}} \right) dz \\ &= -\frac{\mathrm{GDD}(\omega_{sol})}{2{T_0}^2} + \left(\int_0^{2L} k(\omega_{sol}) dz \right) - \omega_{sol} T_{\mathrm{rt}}(\omega_{sol}).\end{aligned} \tag{3}$$

It should be noted that the CEP change is evaluated at a soliton carrier frequency ω_{sol}, which has to be defined such that it captures the linear-optical phase and group delay experienced by the intracavity soliton. For an ideal soliton pulse, the pulse spectrum is symmetric, and the peak frequency arises as a natural choice. In a modelocked laser exhibiting a SFS effect, this frequency ω_{sol} depends on the laser output power. In addition, the soliton dynamics cause T_0 to shorten with increasing P_{avg}. By using partial derivatives w.r.t. ω_{sol} rather than full derivatives (so that the implicit dependencies of ${T_0}^2$ on other system parameters are not included), we can calculate the effect of SFS on the CEP change as:

$$\begin{aligned}\frac{\partial}{\partial \omega_{sol}} \Delta(\phi_{\mathrm{CEP}}) &= -\frac{1}{2{T_0}^2} \frac{\partial \mathrm{GDD}(\omega_{sol})}{\partial \omega_{sol}} + T_{\mathrm{rt}}(\omega_{sol}) - T_{\mathrm{rt}}(\omega_{sol}) - \omega_{sol} \frac{\partial T_{\mathrm{rt}}(\omega_{sol})}{\partial \omega_{sol}} \\ &= -\frac{\mathrm{TOD}(\omega_{sol})}{2{T_0}^2} - \omega_{sol} \cdot \mathrm{GDD}(\omega_{sol}).\end{aligned} \tag{4}$$

Based on this equation, we can identify two mechanisms by which the presence of an SFS affects the CEP. The first coupling mechanism results from cavity roundtrip third-order dispersion (TOD) and the inverse soliton pulse duration squared ($1/{T_0}^2$). The second mechanism arises from GDD and the SFS. These two terms can carry opposite signs, differ in magnitude, and strongly depend on the underlying laser architecture.

3. Characterization of f_{CEO} dynamics

In our recent work [28], we presented a dispersion optimized 10.5-GHz straight-cavity SESAM-modelocked laser and demonstrated self-referenced f_{CEO} –detection without the need of any

Optics EXPRESS

extra-cavity optical amplification. In this work, we used the same 10.5-GHz laser consisting of four elements: an ytterbium-doped $CaGdAlO_4$ (Yb:CALGO) gain crystal, a periodically polled lithium niobite (PPLN) crystal incorporating an apodized two-dimensionally patterned quasi-phase-matching (QPM) grating structure, a single quantum-well SESAM and a curved output coupler (OC) with a multi-functional thin-film coating (Fig. 1).

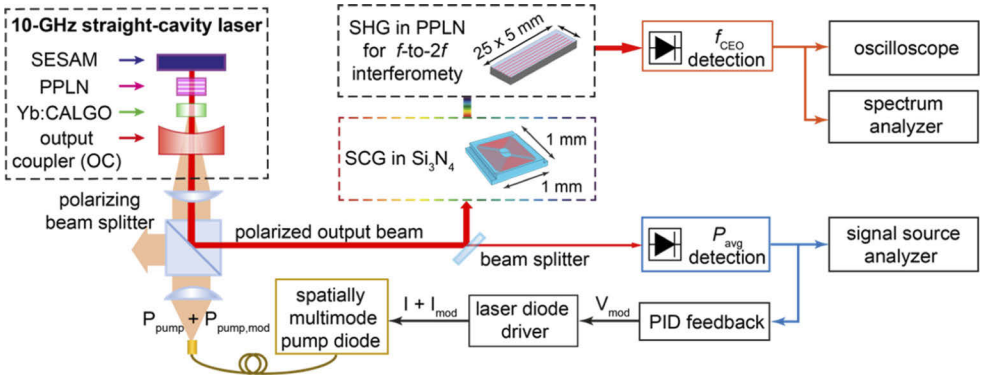

Fig. 1. Experimental setup used to characterize the CEO dynamics of a straight-cavity 10-GHz Yb:CALGO laser, enabled by the use of self-defocusing cascaded quadratic nonlinearity in a PPLN crystal. Supercontinuum generation (SCG) in dispersion-engineered Si_3N_4 waveguides and subsequent f-to-2f interferometry are used for f_{CEO} detection. Simultaneously, the average power (P_{avg}) is detected and used with a proportional-integral-derivative (PID) feedback loop to act on the pump power to stabilize P_{avg}.

In this work, we used a low pulse-energy (29 pJ) platform for self-referenced f_{CEO}-detection enabled by two highly efficient chip-scale waveguides: A Si_3N_4 for SCG and RPE-PPLN for SHG in f-to-2f interferometry. The temporal fluctuations of the f_{CEO} beat-note were measured with an oscilloscope and the radio frequency (RF) spectrum was measured with a spectrum analyzer. Simultaneously, we detected P_{avg} with a free-space reverse-biased photodiode and measured the relative intensity noise (RIN) spectrum with a signal source analyzer. The rest of this section is structured as follows. In section 3.1 we characterize the quasi-static CEO tuning by ramping the pump power and measuring both CEO beat-notes for P_{avg} from 300 mW to 740 mW and compare it with the predicted CEO change from Eq. (5). The dynamic tuning of f_{CEO} (section 3.2) becomes apparent by measuring the transfer function from a modulation voltage (V_{mod}) to pump power ($P_{pump,mod}$), P_{avg} and f_{CEO}. Finally, we show stabilization of P_{avg} with a proportional-integral-derivative (PID) feedback-loop acting on $P_{pump,mod}$, and analyze the noise spectrum of f_{CEO}.

3.1. Static CEO tuning

The self-defocusing cascaded nonlinearity is the key-enabling element of the investigated straight-cavity laser architecture [27,43]. To incorporate CQNs in a laser cavity, it is important to avoid excessive losses from the phase-mismatched SHG process. This can be achieved by adiabatically exciting and deexciting the second harmonic soliton in an apodized quasi-phase-matching (QPM) device [43]. Nonetheless, group velocity mismatch (GVM) between the fundamental soliton and its second-harmonic in the QPM device causes a SFS [44]. In a process somewhat similar to the Raman soliton SFS effect [45], the loss-related part of the CQN response scatters the low-frequency spectral components, which are closer to SHG phase-matching, to the high-frequency part of the spectrum.

Optics EXPRESS

As a result, an asymmetric laser spectrum appears, as shown in Fig. 2(c). This asymmetry raises the question of how to define the correct soliton frequency for use in Eq. (4). A similar question emerges when choosing a carrier frequency to facilitate computationally efficient numerical simulations of ultrashort pulses. The predictions from a model that captures all the relevant effects are invariant w.r.t. the choice of this carrier frequency [46]. However, the correct choice of carrier frequency becomes important when using reduced models. In the context of our experiments, we found that our simple model [Eq. (4)] slightly overestimates the CEP change if the carrier frequency is chosen to be equal to the peak frequency or the centroid frequency (i.e. the center of mass) of the laser power spectrum. Excellent agreement with the experimental data was found if the carrier frequency was defined as the centroid frequency of the electric field amplitude $|\tilde{E}(\omega)|$, corresponding to the square root of the measured laser power spectrum:

$$\omega_{\text{soliton}} = \frac{\int_0^\infty \omega \cdot |\tilde{E}(\omega)| d\omega}{\int_0^\infty |\tilde{E}(\omega)| d\omega}. \tag{5}$$

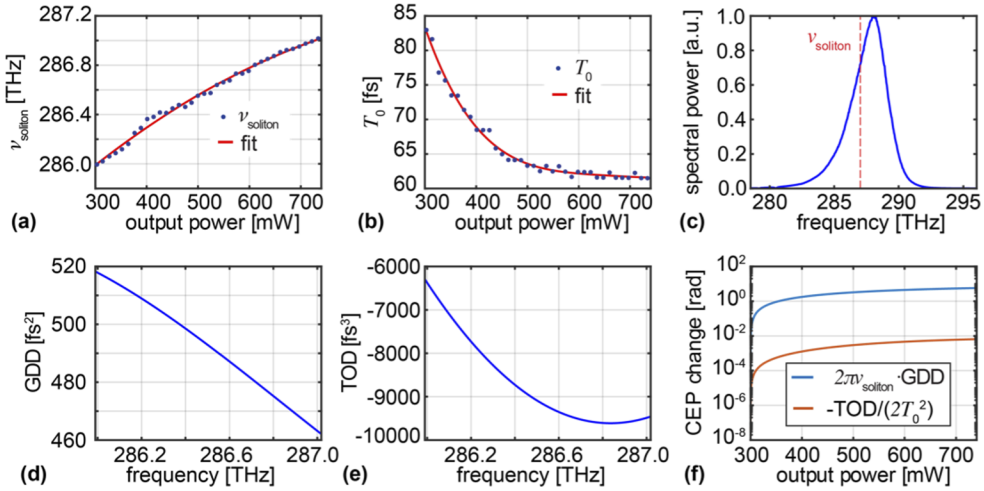

Fig. 2. (a) Measured self-frequency shift (SFS) of soliton frequency ν_{soliton} as a function of laser output power (blue dots) and quadratic polynomial fit. (b) Soliton pulse width (T_0) (Eq. (2)) and fourth-order polynomial fit (red). (c) Normalized spectral power (blue) and soliton angular frequency (ν_{soliton} red dashed) defined as the spectral amplitude's centroid frequency (Eq. (5)) at $P_{\text{avg}} = 623$ mW. (d) cavity roundtrip group delay dispersion (GDD) and (e) third-order dispersion (TOD) as a function of frequency. (f) contribution to the carrier-envelope offset phase (CEP) on a semilogarithmic scale. See **Data File 1** for underlying values.

The effective soliton frequency defined in this equation was calculated for the experimentally measured laser spectra recorded at P_{avg} ranging from 300 mW to 740 mW, and the resulting curve was fitted with a quadratic polynomial (Fig. 2(a)). The soliton pulse duration T_0 initially follows the 1/(power) trend of conventional soliton modelocking but flattens for P_{avg} exceeding 500 mW due to the SFS and the therefore reduced SPM from the PPLN crystal. Therefore, we used a fourth-order polynomial to fit the average power dependence of T_0 (Fig. 2(b)).

The prediction of the SFS-induced CEP change requires precise knowledge of the total cavity roundtrip dispersion. In this laser, the intracavity GDD, the output coupling rate in the range of 1030 nm-1060 nm, and the pump transmission at 980 nm are all managed with a single multi-functional thin-film coating on the curved end mirror. Due to the difficulty of meeting all of these specifications simultaneously, there is a slope in the resulting total cavity round trip

Optics EXPRESS

GDD and TOD. The dispersion of the OC and the SESAM were measured with a home-built white-light interferometer with a spectral resolution of 1 nm. The obtained GDD values were fitted with a fifth-order polynomial. Further, we calculated the dispersion of the 1.5-mm long Yb:CALGO crystal and the 2-mm long PPLN crystal using the Sellmeier equations [47,48] to obtain the total cavity round trip GDD (Fig. 2(d)). The cavity roundtrip TOD was determined by taking the numerical derivative of the GDD (Fig. 2(e)).

We calculated the SFS-induced CEP change as a function of P_{avg} using Eq. (4) and compared the two coupling mechanisms for our laser system (Fig. 2(f)). We found that the GDD induced CEP change exceeds the TOD term by more than two orders of magnitude. Further, the contributions carry an opposite sign, which could result in a turning point of the CEP for laser systems with comparable contributions.

To verify our model, we measured the RF spectrum at a series of output power levels; an example measurement at 623 mW is shown in Fig. 3(a). We then compared the two carrier-envelope offset beat-notes ($f_{CEO,1}$ and $f_{CEO,2} = f_{rep} - f_{CEO,1}$) with expected CEP changes ($f_{CEO,1,model}$ and $f_{CEO,2,model}$) based on Eq. (4), using the experimentally determined power dependence of $\omega_{soliton} = 2\pi \cdot \nu_{soliton}$. Since the model only predicts the rate of change, we set the initial value equal to the first measured beat-note frequency $f_{CEO,1} = f_{CEO,2} = f_{rep}/2$. As shown in Fig. 3(b), our model agrees well for output powers up to 500 mW and slightly underestimates the CEP change above that point. That point also coincides with the power at which the pulse shortening starts to deviate from the expected 1/(power) scaling. Our model predicts that the relatively large SFS present in the laser couples, via intracavity GDD, to the CEP and causes a large shift in the order of 2π over the full output power range from 300 mW to 740 mW.

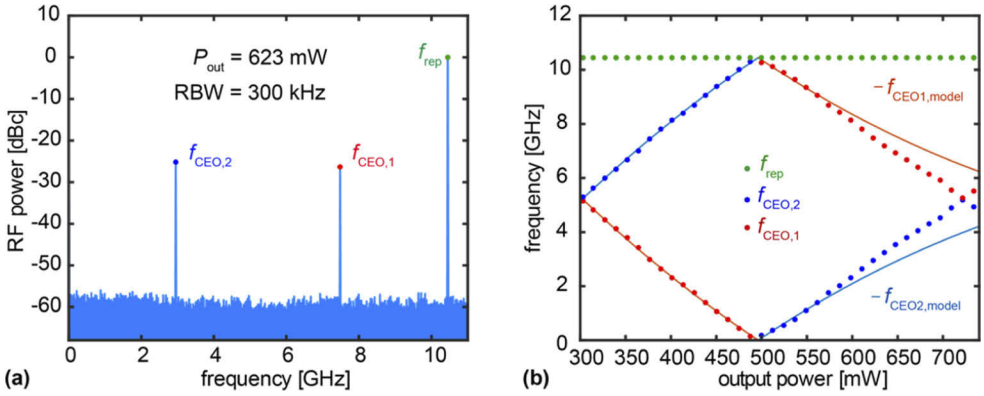

Fig. 3. (a) Exemplary radio frequency (RF) spectrum at $P_{avg} = 623$ mW measured with a resolution bandwidth (RBW) of 300 kHz. The pulse repetition rate (f_{rep}, green circle) and both CEO beat-notes ($f_{CEO,1}$ and $f_{CEO,2}$, blue and red circles) were measured for a series of laser output powers. Predicted CEO ($f_{CEO1,model}$ and $f_{CEO2,model}$) beat-note positions, emerging from the presence of a SFS and intracavity GDD. See **Data File 2** for underlying values.

3.2. *Dynamic CEO tuning*

For many frequency comb applications, it is necessary to lock the comb parameters to stable references. PID feedback loops are widely used for that purpose. The monotonic scaling of f_{CEO} with output power (Fig. 3(b)) fulfills the system requirements for a PID loop. While our model (Eq. (4)) captured the low quasi-static tuning sufficiently well, it does not include laser rate equations or other dynamic phenomena, and hence it does not predict the dynamic response of f_{CEO} to fast pump power (P_{pump}) modulations.

Optics EXPRESS

For this reason, we measured the dynamic response of P_{pump}, P_{avg}, and f_{CEO} to voltage modulations (V_{mod}) on the low-noise laser diode driver (Wavelength Electronics LD2.5CHA). We used a lock-in amplifier with an internal frequency generator (UHFLI Zurich Instruments) for the sinusoidal excitation and demodulation of the quantity of interest. While P_{pump} and P_{avg} could be demodulated directly, we used a frequency discriminator (Miteq FMDM-160/35) to convert changes in f_{CEO} to changes in voltage, centered around zero. The obtained transfer functions for relative amplitude and phase in the range of 10 Hz to 1 MHz are shown in Fig. 4.

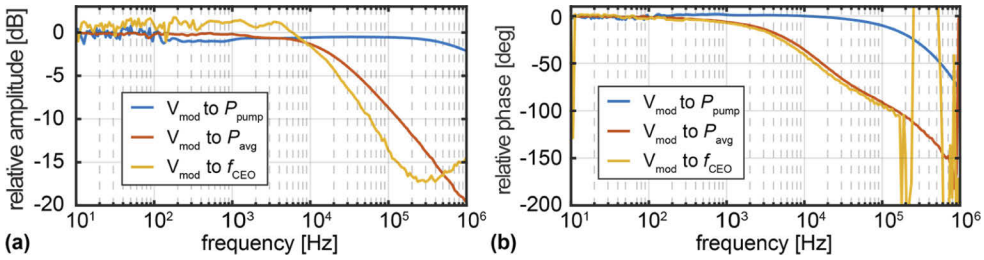

Fig. 4. Transfer functions between laser diode driver modulation voltage V_{mod} and pump power (blue curves), laser average power (orange curves), and f_{CEO} (yellow curves). (a) relative amplitude transfer functions. (b) phase transfer functions. See **Data File 3** for underlying values.

The diode driver can modulate the multimode-fiber-coupled pump diode module up to frequencies exceeding 1 MHz (90° phase shift and 2.4 dB amplitude drop at 1.2 MHz). In contrast, the 420-µs upper-state lifetime of Yb:CALGO [49] introduces a low-pass filter for pump-power modulations resulting in significantly lower modulation bandwidth of P_{avg} (90° phase shift and 8.4 dB amplitude drop at 94 kHz). Similarly, we observed a comparable modulation bandwidth of f_{CEO} (90° phase shift and 11.9 dB amplitude drop at 80 kHz). As P_{avg} strongly influences the CEP via the SFS (Eq. (4)), we expect the dynamic behavior of f_{CEO} and P_{avg} to be strongly correlated.

To further investigate the correlation between P_{avg} and f_{CEO} fluctuations, we stabilized the relative intensity noise (RIN) of our laser and compared the corresponding f_{CEO} fluctuations to the measurements for the free-running laser. We used an average power of 5 mW on a modified commercial InGaAs detector (Thorlabs DET10N2) to reach a shot-noise level below -160 dBc/Hz at frequencies above 1 MHz. We used a PID controller (Vescent Photonics D2-125) to stabilize the obtained detector voltage to its internal voltage reference. The corresponding RIN spectrum was measured out-of-loop using a second photodetector and a signal source analyzer (Agilent E5052B) (Fig. 5(a)). The PID-feedback loop significantly reduced the RIN in the frequency range of 1 kHz to 100 kHz, to a level of −157 dBc/Hz. The RIN-suppressed spectrum crosses the free-running spectrum at a frequency of 300 kHz due to the appearance of a servo bump peaking at around 500 kHz. The noise suppression at frequencies below 1 kHz was compromised by discrete noise frequency components of the voltage reference originating from the 50-Hz power grid frequency and the long airpath (approx. 3 m) between the laser cavity and the photodetector. The feedback loop reduced the integrated rms-RIN (1 Hz – 10 MHz) from 7.7×10^{-5} to 0.7×10^{-5} (Fig. 5(b)).

The frequency noise power spectral density (PSD) of the f_{CEO} beat-note were calculated from time-traces measured with an oscilloscope (Teledyne LeCroy WavePro 254HD, WPHD-2000MPT Option) (Fig. 5(c)). The internal acquisition memory of the oscilloscope imposes a trade-off between sampling rate and trace length. In order to reduce the discretization noise, we chose a high sampling rate of 2.5 GS/s and recorded 800-ms time traces with an analog bandwidth of 2.5 GHz, allowing for frequency noise measurements down to 1.25 Hz. The PSD can be

Optics EXPRESS

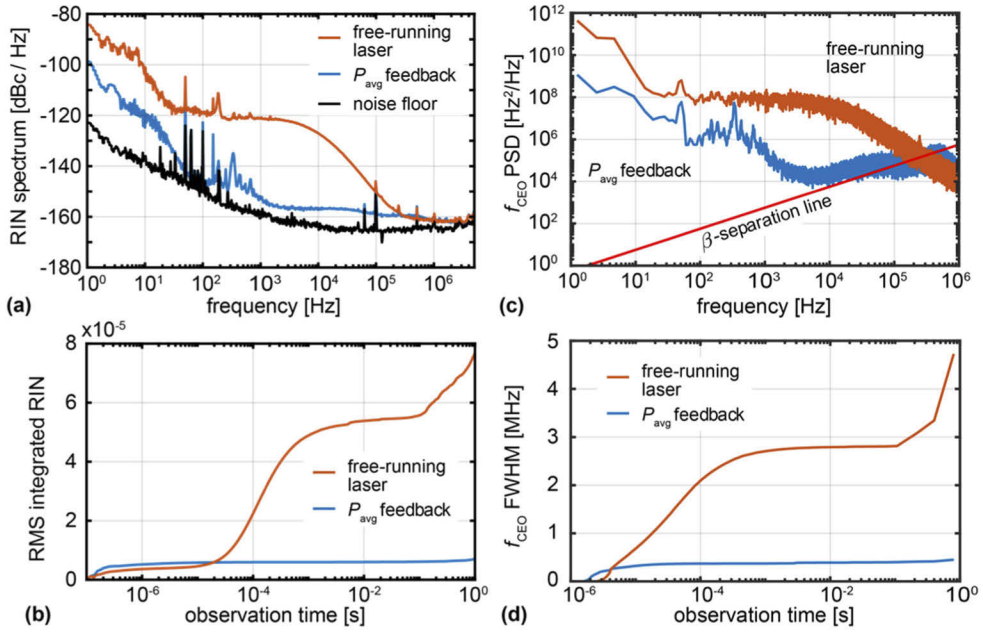

Fig. 5. (a) Relative intensity noise (RIN) spectrum and (b) resulting rms integrated RIN for the case of the free-running laser (orange) and PID-feedback on P_{avg} (blue). (c) Measured power spectral density (PSD) of f_{CEO} fluctuations and (d) estimated f_{CEO} full-width half max linewidth (f_{CEO} FWHM). See **Data File 4** for underlying values.

linked to the CEO-beat note full-width half maximum (FWHM) linewidth via the β-separation line [50]. In this formalism, the frequency noise for a given frequency f only contributes if the corresponding f_{CEO} PSD lies above the β-separation line, *i.e.* if $\mathrm{PSD}_{CEO}(f) > (8\ln(2)/\pi^2)\cdot f$. An estimate of the required feedback bandwidth for locking f_{CEO} to a stable reference can be obtained from the crossing of the free-running f_{CEO} PSD with the β-separation line [50]. For our laser system, the f_{CEO} PSD exceeds the β-separation line up to the crossing point at 300 kHz leading to a broadening of the f_{CEO}-linewidth (Fig. 5(d)). By stabilizing P_{avg} of the laser, we reduced the CEO FWHM linewidth from 4.7 MHz to 0.45 MHz for an observation time of 800 ms.

A tight lock of f_{CEO} is characterized by the reduction of the PSD below the β-separation line, meaning that the noise does not broaden the f_{CEO} linewidth but only contributes to its wings. While the f_{CEO} frequency noise was significantly reduced by the P_{avg} feedback loop, it did not reduce it below the β-separation line. In addition, the increased RIN around the servo bump at 500 kHz leads to an increase in f_{CEO} frequency noise. This servo-bump causes the majority of the CEO-linewidth broadening. Achieving a tight lock of f_{CEO} is complicated by two factors: First, the significant high-frequency noise requires a large feedback bandwidth of at least 300 kHz, compared to the 80 kHz modulation bandwidth. Second, the large initial f_{CEO} linewidth of more than 4 MHz combined with GHz-level carrier frequencies requires a fast phase detector with a large demodulation bandwidth. Further, fast short-term and large long-term drifts of f_{CEO} can easily deregulate a PID feedback loop. While we showed that a significant part of f_{CEO} noise is caused by P_{avg} fluctuations, we cannot rule out other effects independent of pump power.

Our findings indicate five possible strategies for achieving a tight lock of f_{CEO} in a modified laser design based on CQN: First, the SFS-induced coupling between RIN and f_{CEO}-noise could be reduced by using a different material platform with a smaller GVM for the implementation

Optics EXPRESS

of CQN. Second, the SFS-induced coupling could be reduced by lowering intracavity GDD and TOD via optimized dispersion coatings. Third, the RIN could be further reduced by using a higher power photodetection for a lower shot-noise limit in combination with a lower noise voltage reference and PID-feedback loop. Fourth, the f_{CEO} modulation bandwidth could be increased by switching to a shorter lifetime gain material. Lastly, the electronic and frequency noise requirements could be greatly reduced by lowering the pulse-repetition rate of the laser system. Despite the significant challenges involved in achieving a fully stabilized OFC based on CQN, they represent a unique platform offering a large degree of tuning that can be used for spectral interleaving techniques including dual-comb measurements.

4. Conclusion

In this paper, we have investigated analytically and experimentally the effect of a self-frequency shift effect on the carrier-envelope offset frequency in a modelocked 10-GHz straight-cavity laser based on cascaded quadratic nonlinearities.

In the first part, we have developed a simple analytical model to describe the quasi-static dependence of f_{CEO} on average laser output power in the presence of an SFS effect. We found that the SFS couples via the intracavity GDD to the carrier-envelope offset phase, leading to a large phase shift in the order of 2π over an output power range of 300 mW to 740 mW. This effect can be used to freely tune f_{CEO} from zero to the pulse repetition rate frequency of 10.5 GHz.

In the second part, we experimentally investigate the static and dynamic f_{CEO} dependence on average power. We find good agreement between our model and the observed static f_{CEO} tuning. Moreover, we have measured the transfer function from pump current modulation to pump power, laser power, and f_{CEO}. The observed low-pass behavior with a characteristic 90° phase shift and 11.9 dB amplitude drop around 80 kHz for the case of f_{CEO} is caused by the upper-state lifetime of the Yb:CALGO gain material. From the measured free-running f_{CEO} frequency noise, we have estimated a minimum required locking bandwidth of 300 kHz. Finally, we demonstrated that the f_{CEO} frequency noise is reduced up to four orders of magnitude at kHz-frequencies by stabilizing the laser's relative intensity noise to the −157 dBc/Hz level (compared to free-running -120 dBc/Hz), validating the strong coupling predicted by our model. Our results provide the basis for developing the next generation of versatile, high repetition rate, and low-noise optical frequency combs from modelocked lasers based on CQN.

Funding. Schweizerischer Nationalfonds zur Förderung der Wissenschaftlichen Forschung (40B2-0_180933); Eidgenössische Technische Hochschule Zürich (ETH-49 18-1).

Acknowledgments. The authors acknowledge the support of Dr. Benjamin Willenberg for electronic noise optimization of the laser system.

Disclosures. The authors declare no conflicts of interest.

Data availability. Data underlying the results presented in this paper are available in Ref. [51].

References

1. H. R. Telle, G. Steinmeyer, A. E. Dunlop, J. Stenger, D. H. Sutter, and U. Keller, "Carrier-envelope offset phase control: A novel concept for absolute optical frequency measurement and ultrashort pulse generation," Appl. Phys. B **69**(4), 327–332 (1999).
2. D. J. Jones, S. A. Diddams, J. K. Ranka, A. Stentz, R. S. Windeler, J. L. Hall, and S. T. Cundiff, "Carrier-Envelope Phase Control of Femtosecond Mode-Locked Lasers and Direct Optical Frequency Synthesis," Science **288**(5466), 635–639 (2000).
3. A. Apolonski, A. Poppe, G. Tempea, C. Spielmann, T. Udem, R. Holzwarth, T. W. Hänsch, and F. Krausz, "Controlling the Phase Evolution of Few-Cycle Light Pulses," Phys. Rev. Lett. **85**(4), 740–743 (2000).
4. G. J. Spühler, L. Krainer, S. C. Zeller, C. Erny, R. Paschotta, K. J. Weingarten, and U. Keller, "Compact low-noise pulse generating lasers with repetition rates of 10 to 50 GHz," Int. J. High Speed Electron. Syst. **15**(03), 497–512 (2005).
5. A. Bartels, D. Heinecke, and S. A. Diddams, "Passively mode-locked 10 GHz femtosecond Ti:sapphire laser," Opt. Lett. **33**(16), 1905–1907 (2008).

Optics EXPRESS

6. M. Endo, I. Ito, and Y. Kobayashi, "Direct 15-GHz mode-spacing optical frequency comb with a Kerr-lens mode-locked Yb:Y_2O_3 ceramic laser," Opt. Express **23**(2), 1276–1282 (2015).
7. H.-W. Chen, G. Chang, S. Xu, Z. Yang, and F. X. Kärtner, "3 GHz, fundamentally mode-locked, femtosecond Yb-fiber laser," Opt. Lett. **37**(17), 3522–3524 (2012).
8. A. Klenner, M. Golling, and U. Keller, "High peak power gigahertz Yb:CALGO laser," Opt. Express **22**(10), 11884 (2014).
9. S. Kimura, S. Tani, and Y. Kobayashi, "Kerr-lens mode locking above a 20 GHz repetition rate," Optica **6**(5), 532 (2019).
10. M. Mangold, C. A. Zaugg, S. M. Link, M. Golling, B. W. Tilma, and U. Keller, "Pulse repetition rate scaling from 5 to 100 GHz with a high-power semiconductor disk laser," Opt. Express **22**(5), 6099–6107 (2014).
11. S. A. Diddams, L. Hollberg, and V. Mbele, "Molecular fingerprinting with the resolved modes of a femtosecond laser frequency comb," Nature **445**(7128), 627–630 (2007).
12. J. Mandon, G. Guelachvili, and N. Picqué, "Fourier transform spectroscopy with a laser frequency comb," Nat. Photonics **3**(2), 99–102 (2009).
13. R. A. McCracken, J. M. Charsley, and D. T. Reid, "A decade of astrocombs: recent advances in frequency combs for astronomy [Invited]," Opt. Express **25**(13), 15058–15078 (2017).
14. T. M. Fortier, A. Bartels, and S. A. Diddams, "Octave-spanning Ti:sapphire laser with a repetition rate >1 GHz for optical frequency measurements and comparisons," Opt. Lett. **31**(7), 1011–1013 (2006).
15. M. Endo, T. D. Shoji, and T. R. Schibli, "Ultralow Noise Optical Frequency Combs," IEEE J. Sel. Top. Quantum Electron. **24**(5), 1–13 (2018).
16. D. Waldburger, A. S. Mayer, C. G. E. Alfieri, J. Nürnberg, A. R. Johnson, X. Ji, A. Klenner, Y. Okawachi, M. Lipson, A. L. Gaeta, and U. Keller, "Tightly locked optical frequency comb from a semiconductor disk laser," Opt. Express **27**(3), 1786 (2019).
17. S. M. Link, A. Klenner, M. Mangold, C. A. Zaugg, M. Golling, B. W. Tilma, and U. Keller, "Dual-comb modelocked laser," Opt. Express **23**(5), 5521–5531 (2015).
18. T. Ideguchi, T. Nakamura, Y. Kobayashi, and K. Goda, "Kerr-lens mode-locked bidirectional dual-comb ring laser for broadband dual-comb spectroscopy," Optica **3**(7), 748–753 (2016).
19. S. Mehravar, R. A. Norwood, N. Peyghambarian, and K. Kieu, "Real-time dual-comb spectroscopy with a free-running bidirectionally mode-locked fiber laser," Appl. Phys. Lett. **108**(23), 231104 (2016).
20. R. Liao, H. Tian, W. Liu, R. Li, Y. Song, and M. Hu, "Dual-comb generation from a single laser source: principles and spectroscopic applications towards mid-IR—A review," J. Phys. Photonics **2**(4), 042006 (2020).
21. S. Schiller, "Spectrometry with frequency combs," Opt. Lett. **27**(9), 766 (2002).
22. I. Coddington, N. Newbury, and W. Swann, "Dual-comb spectroscopy," Optica **3**(4), 414–426 (2016).
23. S. M. Link, D. J. H. C. Maas, D. Waldburger, and U. Keller, "Dual-comb spectroscopy of water vapor with a free-running semiconductor disk laser," Science **356**(6343), 1164–1168 (2017).
24. P. Jacquet, J. Mandon, B. Bernhardt, R. Holzwarth, G. Guelachvili, T. W. Hänsch, and N. Picqué, "Frequency Comb Fourier Transform Spectroscopy with kHz Optical Resolution," in *Advances in Imaging* (OSA, 2009), p. FMB2.
25. Y.-D. Hsieh, Y. Iyonaga, Y. Sakaguchi, S. Yokoyama, H. Inaba, K. Minoshima, F. Hindle, T. Araki, and T. Yasui, "Spectrally interleaved, comb-mode-resolved spectroscopy using swept dual terahertz combs," Sci. Rep. **4**(1), 3816 (2015).
26. N. Picqué and T. W. Hänsch, "Frequency comb spectroscopy," Nat. Photonics **13**(3), 146–157 (2019).
27. A. S. Mayer, C. R. Phillips, and U. Keller, "Watt-level 10-gigahertz solid-state laser enabled by self-defocusing nonlinearities in an aperiodically poled crystal," Nat. Commun. **8**(1), 1673 (2017).
28. L. M. Krüger, A. S. Mayer, Y. Okawachi, X. Ji, A. Klenner, A. R. Johnson, C. Langrock, M. M. Fejer, M. Lipson, A. L. Gaeta, V. J. Wittwer, T. Südmeyer, C. R. Phillips, and U. Keller, "Performance scaling of a 10-GHz solid-state laser enabling self-referenced CEO frequency detection without amplification," Opt. Express **28**(9), 12755–12770 (2020).
29. G. I. Stegeman, D. J. Hagan, and L. Torner, "$\chi^{(2)}$ cascading phenomena and their applications to all-optical signal processing, mode-locking, pulse compression and solitons," Opt. Quantum Electron. **28**(12), 1691–1740 (1996).
30. F. X. Kärtner, I. D. Jung, and U. Keller, "Soliton mode-locking with saturable absorbers," IEEE J. Sel. Top. Quantum Electron. **2**(3), 540–556 (1996).
31. D. N. Christodoulides, I. C. Khoo, G. J. Salamo, G. I. Stegeman, and E. W. Van Stryland, "Nonlinear refraction and absorption: mechanisms and magnitudes," Adv. Opt. Photonics **2**(1), 60 (2010).
32. C. Hönninger, R. Paschotta, F. Morier-Genoud, M. Moser, and U. Keller, "Q-switching stability limits of continuous-wave passive mode locking," J. Opt. Soc. Am. B **16**(1), 46–56 (1999).
33. A. Klenner and U. Keller, "All-optical Q-switching limiter for high-power gigahertz modelocked diode-pumped solid-state lasers," Opt. Express **23**(7), 8532 (2015).
34. U. Keller, K. J. Weingarten, F. X. Kartner, D. Kopf, B. Braun, I. D. Jung, R. Fluck, C. Honninger, N. Matuschek, and J. Aus der Au, "Semiconductor saturable absorber mirrors (SESAM's) for femtosecond to nanosecond pulse generation in solid-state lasers," IEEE J. Sel. Top. Quantum Electron. **2**(3), 435–453 (1996).
35. A. R. Johnson, A. S. Mayer, A. Klenner, K. Luke, E. S. Lamb, M. R. E. Lamont, C. Joshi, Y. Okawachi, F. W. Wise, M. Lipson, U. Keller, and A. L. Gaeta, "Octave-spanning coherent supercontinuum generation in a silicon nitride waveguide," Opt. Lett. **40**(21), 5117–5120 (2015).

Optics EXPRESS

36. K. R. Parameswaran, R. K. Route, J. R. Kurz, R. V. Roussev, M. M. Fejer, and M. Fujimura, "Highly efficient second-harmonic generation in buried waveguides formed by annealed and reverse proton exchange in periodically poled lithium niobate," Opt. Lett. **27**(3), 179–181 (2002).
37. F. W. Helbing, G. Steinmeyer, U. Keller, R. S. Windeler, J. Stenger, and H. R. Telle, "Carrier-envelope offset dynamics of mode-locked lasers," Opt. Lett. **27**(3), 194–196 (2002).
38. K. W. Holman, R. J. Jones, A. Marian, S. T. Cundiff, and J. Ye, "Detailed studies and control of intensity-related dynamics of femtosecond frequency combs from mode-locked Ti:sapphire lasers," IEEE J. Sel. Top. Quantum Electron. **9**(4), 1018–1024 (2003).
39. N. R. Newbury and B. R. Washburn, "Theory of the frequency comb output from a femtosecond fiber laser," IEEE J. Quantum Electron. **41**(11), 1388–1402 (2005).
40. L. Matos, O. D. Mücke, J. Chen, and F. X. Kärtner, "Carrier-envelope phase dynamics and noise analysis in octave-spanning Ti:sapphire lasers," Opt. Express **14**(6), 2497–2511 (2006).
41. F. W. Helbing, G. Steinmeyer, J. Stenger, H. R. Telle, and U. Keller, "Carrier–envelope-offset dynamics and stabilization of femtosecond pulses," Appl. Phys. B **74**(S1), s35–s42 (2002).
42. Govind P. Agrawal, *Nonlinear Fiber Optics*, 5th ed. (Academic Press, 2013).
43. C. R. Phillips, A. S. Mayer, A. Klenner, and U. Keller, "Femtosecond mode locking based on adiabatic excitation of quadratic solitons," Optica **2**(8), 667 (2015).
44. F. Ö. Ilday, K. Beckwitt, Y.-F. Chen, H. Lim, and F. W. Wise, "Controllable Raman-like nonlinearities from nonstationary, cascaded quadratic processes," J. Opt. Soc. Am. B **21**(2), 376 (2004).
45. J. P. Gordon, "Theory of the soliton self-frequency shift," Opt. Lett. **11**(10), 662 (1986).
46. M. Kolesik and J. V. Moloney, "Nonlinear optical pulse propagation simulation: From Maxwell's to unidirectional equations," Phys. Rev. E **70**(3), 036604 (2004).
47. P. Loiko, P. Becker, L. Bohatý, C. Liebald, M. Peltz, S. Vernay, D. Rytz, J. M. Serres, X. Mateos, Y. Wang, X. Xu, J. Xu, A. Major, A. Baranov, U. Griebner, and V. Petrov, "Sellmeier equations, group velocity dispersion, and thermo-optic dispersion formulas for CaLnAlO$_4$ (Ln = Y, Gd) laser host crystals," Opt. Lett. **42**(12), 2275–2278 (2017).
48. O. Gayer, Z. Sacks, E. Galun, and A. Arie, "Temperature and wavelength dependent refractive index equations for MgO-doped congruent and stoichiometric $LiNbO_3$," Appl. Phys. B **91**(2), 343–348 (2008).
49. J. Petit, P. Goldner, and B. Viana, "Laser emission with low quantum defect in Yb:$CaGdAlO_4$," Opt. Lett. **30**(11), 1345 (2005).
50. G. D. Domenico, S. Schilt, and P. Thomann, "Simple approach to the relation between laser frequency noise and laser line shape," Appl. Opt. **49**(25), 4801–4807 (2010).
51. L. M. Krüger, S. L. Camenzind, C. R. Phillips, and U. Keller, "Supplementary document for Carrier-envelope offset frequency dynamics of a 10-GHz modelocked laser based on cascaded quadratic nonlinearities," (2021).